2022 IEEE/ASME International Conference on
Advanced Intelligent Mechatronics (AIM)

Microfluidic device for analysis of magnetorheological fluids' properties

Timothy Loayza[1], Sofia Lydia Ntella[1], Pooneh Mohaghegh[1], Christian Koechli[1], Yves Perriard[1]

2022 IEEE/ASME International Conference on Advanced Intelligent Mechatronics (AIM) | 978-1-6654-1308-4/22/$31.00 ©2022 IEEE | DOI: 10.1109/AIM52237.2022.9863248

***Abstract*— The valve mode is the most common operational mode of magnetorheological fluid (MRF) devices in engineering applications. Magnetorheological (MR) valves have been studied upon their self-sensing capabilities resulting from the electromagnetic induction phenomenon. In parallel, studies have been carried out regarding the microstructural properties and the analytical modeling of MRFs used in valves. This paper presents the design and fabrication of a microfluidic system in the form of a magnetic circuit, consisting of a MRF flow channel, with dimensions close to those of previously studied miniaturized MR valves. The channel is enclosed in ferromagnetic and transparent sheets. The sheets facilitate the magnetic field distribution, created by a coil. The channel allows the microscopical MRF particles observation and their correlation with the MRF magnetic and rheological properties when the self-sensing phenomenon occurs.**

***Index Terms*— Magnetorheological fluid, microfluidic device, self-sensing MR valves**

I. INTRODUCTION

MRFs are smart materials with rheological properties that are altered rapidly with the application of a magnetic field. They are considered non-Newtonian fluids and consist of micro-meter-sized iron particles, suspended in a carrier medium, such as oil. Jacob Rabinow obtained the first patent of MRFs in 1948 [1]. However, nowadays, MRFs still attract the attention of many researchers, due to their fast response, high controllability, and low power consumption properties, as well as the simple interfaces needed between the electrical power input and the mechanical power output [2]. A large variety of industrial applications of MRFs includes gripping and handling devices [3],[4], applications in the automotive industry [5], and haptic devices [6].

The most frequently used systems using MRFs are valves [7], which include a fluidic circuit through which the MRF flows. A valve can be closed by applying a magnetic field to the MRF that flows in it, increasing its viscosity and preventing it from flowing. The valve is open by default, as the MRF has a low viscosity if no magnetic field is applied [8]. In our previous studies, we presented the design of a miniaturized MR valve that enables its self-sensing capabilities with regard to pressure and flow rate [9],[10]. This is achieved because the MRFs undergo a change in their magnetic properties, when pressure is applied to them or when their flow rate is changed, leading to electromagnetic induction phenomena. The goal of these studies was the creation of a MR device with two functionalities, either working as a traditional MR valve or working as a pressure or flow rate sensor.

[1]The authors are with the Integrated Actuators Laboratory (LAI), École Polytechnique Fédérale de Lausanne (EPFL), Neuchâtel, Switzerland sofia.ntella@epfl.ch

The approach of the previous papers focuses on the observation and study of the result of the MRF properties variation, which is the induced voltage. However, no study has been performed on the microscopical behaviour of the MRF that results in the aforementioned phenomenon. Up to now, researchers also showed the link between the rheological properties of the MRF and the geometrical distribution of the ferromagnetic particles in it [11]. This was studied via the measurement of the MRF yield stress and the observation of the agglomeration of the MRF ferromagnetic particles in function of the applied magnetic field. The studies concluded that the presence of magnetic field triggered the agglomeration of the particles in the MRF, a fact responsible for the increase of MRF viscosity.

To explore the microscopical behaviour of the MRF, past studies have mainly used bright field microscopy [12], [13]. Their observations revealed the variation in the distribution of ferromagnetic particles in the MRF if a magnetic field was applied to the fluid [14]. In order to perform the measurements, different setups have been developed and used, but most of them were using a Polydimethylsiloxane (PDMS) microchannel with a magnetic circuit surrounding it, to apply the magnetic field on the MRF [12], [13].

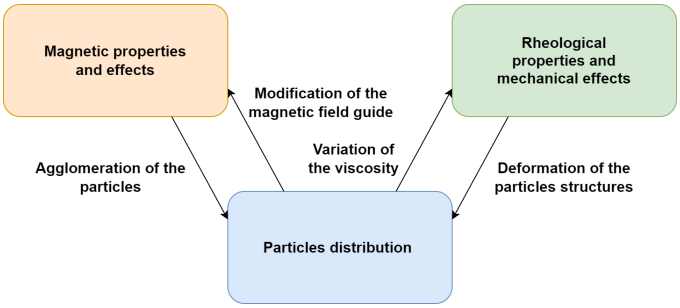

Fig. 1. Links between the rheological properties, the distribution of the particles and the magnetic properties of the MRF.

In the current work, the variations of the MRF magnetic properties are studied with a measurement setup similar to a valve. The setup can reproduce the magnetic field creation and the electromagnetic induction phenomenon with the use of two coils, as well as the fluid flow in a micro-meter-sized channel and the pressure measurement. Its size and fabrication methods allow, in parallel, the MRF observation under an optical microscope, while the magnetic and flow phenomena occur. The MRF is studied using a transparent microchannel with the dark-field microscopy technique [15]. The enhancement of the spatially high-frequency details detection provided by the latter

technique [16] is crucial for the discrimination of the particles and is the main reason that led to the choice of this technique. In comparison with previous works, the presented one proposes a microfluidic device that reveals for the first time the links between the rheological, the magnetic properties of the MRF and the geometrical distribution of the particles, as shown in Fig. 1. This allows a deeper understanding of the induction phenomena appearing in the MRF that is enclosed in a valve, enabling future development of fully bi-functional MR devices as valves or as pressure sensors.

II. MATERIALS & METHODS

A. Self-sensing MR valve modeling

MR valves are constituted of a ferromagnetic core around which an exciting coil is wound, as shown in Fig. 2(a). The ferromagnetic core contains a gap through which the MRF passes and in which the MRF is exposed to a magnetic field B. This exposure triggers an alignment of the particles inside the MRF and leads to the creation of chain-like structures from one side of the gap to the other. In that event, the fluid state is shifted from liquid to semi-solid, leading macroscopically to a variation of the MRF viscosity.

The goal of the current paper is to study the properties of the MRF microscopically. This is not possible in the closed environment of the cylindrical MR valve structure, where the valve is covered and no access to the microscope is allowed. Thus, we created a setup that can simulate the conditions of the MRF in the gap of the valve described previously, as well as of the influence of the magnetic field, pressure drop, and flow on the fluid. Fig. 2(b) represents the schematics of the measurement device. A rectangular magnetic circuit is created with ferromagnetic material while a gap with width g is the point under observation with the microscope. The gap is filled with MRF and a magnetic field is created with a coil. The dimensions of the proposed setup are presented in Table I. The MRF used in the setup is a dilution of the MRF-132DG [17] down to a 2% volume-on-volume ratio of ferromagnetic particles.

Fig. 2(c) depicts the magnetic lumped element model of the measurement device. When a DC current is applied to the exciting coil, a magnetic potential Θ is applied to the magnetic circuit of the valve and leads to the creation of a magnetic flux Φ. This results in the reversible formation of chains of particles in the gap. This variation of the distribution of the particles leads to the change in the magnetic properties of the MRF and of the magnetic flux Φ in the magnetic circuit for a constant magnetic potential Θ. In order to sense the variation of the magnetic flux Φ in the magnetic circuit, a second coil named the sensing coil is wound around the iron core.

As reported in the literature, the permeance Λ_{mrf} associated with a MRF is not constant. It varies with several parameters like the pressure applied to it or the flow rate of the MRF [9] [10]. In order to measure the variation of the magnetic properties of the MRF, the variation of the magnetic flux Φ is measured through the induced voltage V_i on the sensing coil of Fig. 2(b).

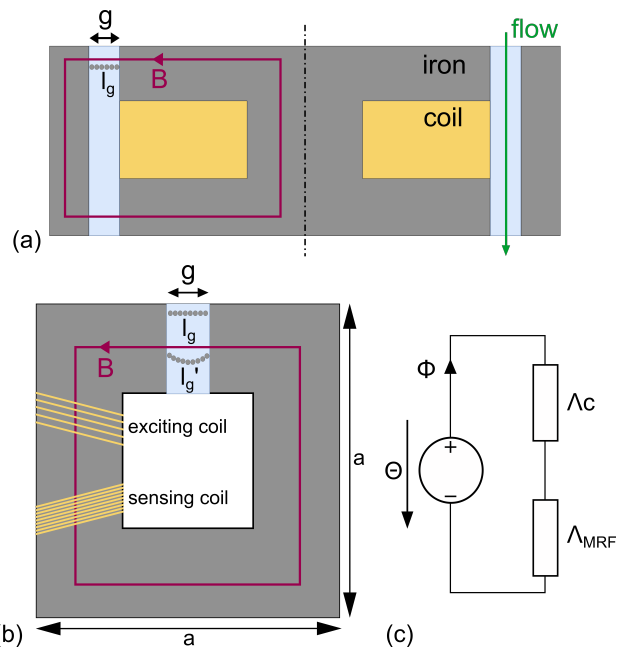

Fig. 2. (a) Planar cross-section of MR valve (b) Schematics of the measurement setup (c) Magnetic lumped element model of the measurement setup.

TABLE I
MEASUREMENT DEVICE CHARACTERISTICS

Quantity	Value
g	1 mm
w	20 mm
h	1.5 mm
a	60 mm
N_e	51 turns
N_s	193 turns
μ_{iron}	1000

The electrical circuit depicted in Fig. 3 shows the exciting circuit on the left part with the power source which provides a voltage V and a DC current i, the circuit resistance R_c, and the resistance of the exciting coil R_e. The magnetic circuit inductance L is not constant and is equal to $N_e^2\Lambda$, where Λ is the permeance of the magnetic circuit. On the right side, the sensing circuit is represented with the sensing coil, and a measurement device for the induced voltage. In our case, we made use of a WAVERUNNER LT224 LeCroy digital oscilloscope, which has a gain of 10'000. The gain is obtained with two INA110KP amplifiers in series. The electrical equations for the exciting and sensing circuits are given below:

$$V = (R_c + R_e) \cdot i + \frac{d\Psi_e}{dt} = (R_c + R_e) \cdot i + \frac{d(L \cdot i)}{dt} \quad (1)$$

$$V_i = \frac{d\Psi_s}{dt} = N_s \frac{d\Phi}{dt} \quad (2)$$

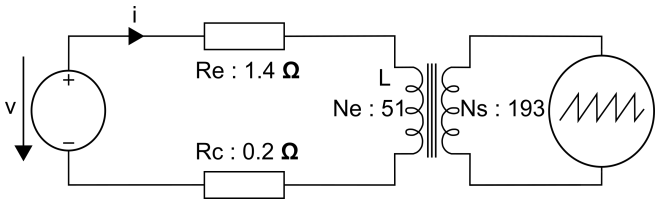

Fig. 3. Electrical lumped element model of the measuring circuit including the exciting coil and the sensing coil.

The magnetic circuit depicted in Fig. 2(c) contains the source of magnetic potential Θ provided by the exciting coil, the magnetic flux Φ, the permeance of the circuit Λ_c and the permeance of the gap which is filled with MRF Λ_{mrf}. The latter is not constant, as the magnetic properties of the MRF are not constant, which leads to the calculation of a non-constant relative permeability of the MRF μ_{mrf}. The magnetic equations are given below:

$$\Lambda_c = \mu_0 \mu_{iron} \frac{S}{l_{iron}} \tag{3}$$

$$\Lambda_{mrf} = \mu_0 \mu_{mrf} \frac{S}{g} \tag{4}$$

$$\Lambda = (\frac{1}{\Lambda_c} + \frac{1}{\Lambda_{mrf}})^{-1} = \frac{\Lambda_c \Lambda_{mrf}}{\Lambda_c + \Lambda_{mrf}} \tag{5}$$

$$\Phi = \Theta \cdot \Lambda = N_e \cdot i \cdot \Lambda \tag{6}$$

where S is the cross-section of the ferromagnetic core and is equal to $w \cdot h$ (h is the thickness of the ferromagnetic core) and l_{iron} is the length of the magnetic field path in the ferromagnetic core and is equal to $4(a-w)-g$. Therefore, the induced voltage on the sensing coil is calculated below with the equations 2, 5, and 6 and with a constant current i.

$$\frac{d\Lambda}{dt} = \frac{\Lambda_c^2}{(\Lambda_c + \Lambda_{mrf})^2} \cdot \frac{d\Lambda_{mrf}}{dt} \tag{7}$$

$$V_i = N_s \frac{d\Phi}{dt} = N_s N_e i \cdot \frac{\Lambda_c^2}{(\Lambda_c + \Lambda_{mrf})^2} \cdot \frac{d\Lambda_{mrf}}{dt} \tag{8}$$

$$V_i = N_s N_e i \cdot \frac{\Lambda_c^2}{(\Lambda_c + \Lambda_{mrf})^2} \cdot \mu_0 \frac{S}{g} \cdot \frac{d\mu_{mrf}}{dt} \tag{9}$$

Furthermore, to calculate the change of relative permeability of the MRF μ_{mrf} from the time t_0 to t_1, an integration can be performed on the induced voltage. Thus the variation of the relative permeability of the MRF can be obtained with the measured induced voltage.

$$\int_{t_0}^{t_1} V_i \, dt = N_s N_e i \cdot \frac{\Lambda_c^2}{(\Lambda_c + \Lambda_{mrf})^2} \cdot \mu_0 \frac{S}{g} \cdot \Delta\mu_{mrf} \tag{10}$$

In order to approximate the relative permeability μ_{mrf} of the diluted MRF used in the setup, the Maxwell-Garnett rule [18], depicted in equation 11, was used. The relative permeability of the medium μ_m is the one of the silicon oil and is equal to 1, the relative permeability of the particles μ_p is the one of the iron μ_{iron} and the volume on volume ratio ν_p of the particles is 2%. Furthermore, the Maxwell-Garnett rule assumes a good dispersion of the particles in the medium, which is not the case when the particles are agglomerated in chain-like clusters but can be assumed when the chains of particles are broken by applied pressure.

$$\mu_{mrf} = \mu_m \frac{\mu_p(1+2\nu_p) - \mu_m(2\nu_p - 2)}{\mu_m(2+\nu_p) + \mu_p(1-\nu_p)} \tag{11}$$

The different values of the variables can be then calculated (Table II).

TABLE II
MEASUREMENT DEVICE CALCULATED VALUES

Quantity	Value
μ_{mrf}	1.061
S	30 mm^2
l_{iron}	159 mm
Λ_c	$2.37{\cdot}10^{-7}$ Tm^2/A
Λ_{mrf}	$4.00{\cdot}10^{-8}$ Tm^2/A

B. Microfluidic device design and fabrication

Historically, microfluidic devices are fabricated to perform biological assays. For these applications, the device can be used to trap or sort cells based on their mechanical, physical, and even chemical properties in some use cases [19]. In our case, the device will serve the purpose of reconstructing the micrometer-sized channel of the miniaturized MR valves, allowing the observations under the microscope. The steps of the device fabrication are presented below.

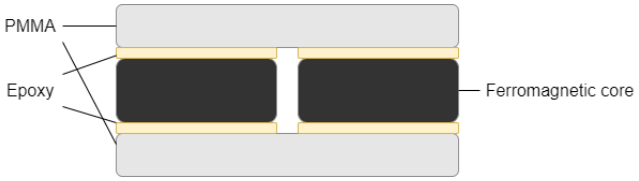

Fig. 4. Front view of the microscopy device with the different layers.

The microscopy device was fabricated using two plates of Polymethyl Methacrylate (PMMA), which were glued on the top and bottom of the ferromagnetic core with epoxy, as depicted in Fig. 4. Furthermore, in order to connect the microchannel to the fluidic circuit, Mini Luer to pipette adapters had to be glued together with microfluidic pipes to the inlet, and outlet of the microchannel with epoxy. Several problems had to be overcome in order to perform the measurements: firstly, the bonding of the glue on the materials had to seal the whole channel without leakages; secondly, the gluing had to be accomplished on a large surface to maximize the strength of the bond in order to sustain the pressure in the channel,

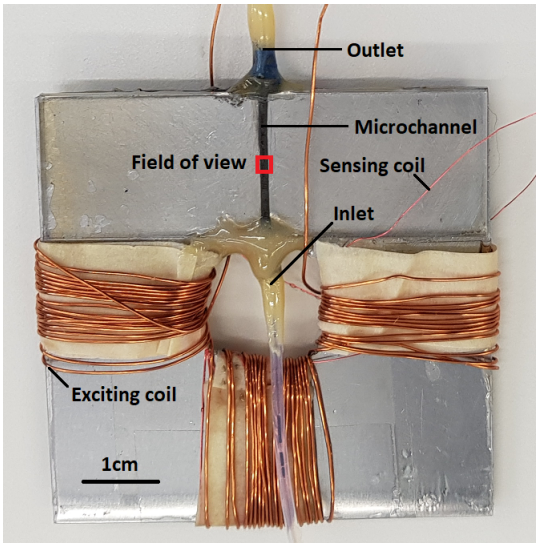

Fig. 5. Fabricated measurement device with one exciting coil, one sensing coil and a microchannel for the MRF to pass through.

which was as high as 10 bars; thirdly, the epoxy must not flow in the channel, to avoid clogging it. To complete the setup, a $250\mu L$ syringe was used to pressurize the fluid and a pressure sensor MS583730BA01-50 was positioned after the syringe to measure the applied pressure.

Fig. 5 is a picture of the fabricated device, including the sensing coils, inlet and outlet of the channel as well as the point in the middle of the flow channel, which was placed under the microscope to perform the observations.

III. RESULTS & DISCUSSION

As explained in the previous chapters, the MR valve functions in two states. In the open state, where the current on the coil is off, there is no magnetic field applied on the MRF, thus it can flow freely in the valve. In the closed state, a current flows in the exciting coil and generates a magnetic field which is applied on the MRF. This field causes a magnetic force on the ferromagnetic particles in order to optimize the path of the magnetic field in the gap, which is filled with MRF. Thus, the ferromagnetic particles in the microchannel form chains, which are preventing any flow, until a certain pressure is applied and breaks them. During the measurements, the valve is in the closed state and a sudden peak of pressure is applied on the microchannel of the valve. This leads to the breakage of the particles' structures and the creation of a flow during the application of the pressure. During this time, the pressure is measured and recorded with an Arduino Leonardo. The induced voltage created by the variation of the magnetic properties of the MRF is measured with an oscilloscope. Additionally, a 1.6 mm section of the microchannel is filmed with the microscope, using the dark field microscopy technique. These data are then used to show the relationship between the distribution of particles in the MRF and its magnetic properties. The measurements are filtered with a 50Hz cut-off frequency Gaussian filter, because the noise ratio is high during the measurement, due to the electromagnetic perturbation of the environment and the double stage amplification.

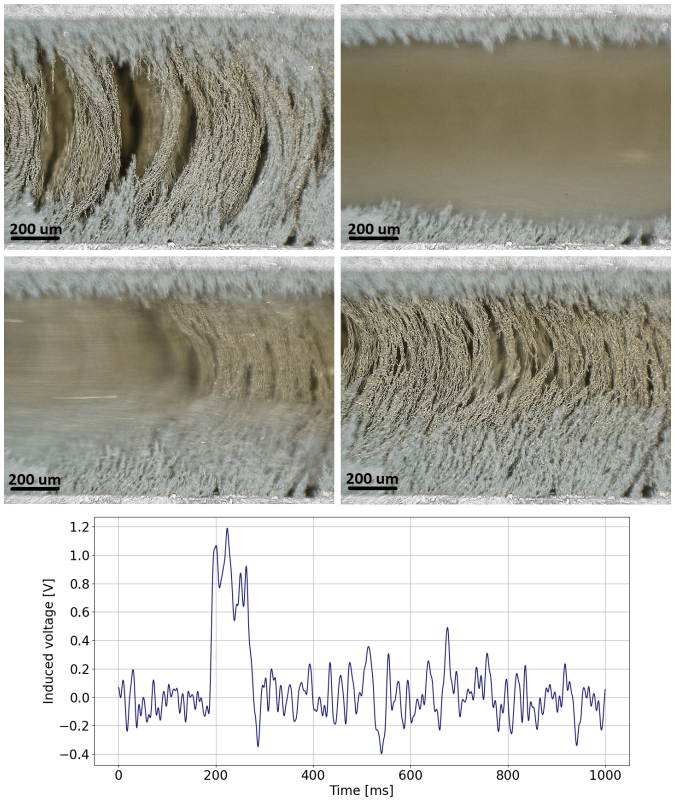

Fig. 6. Four frames of a video separated by 67ms each, which show the breaking of the chains of particles in the microchannel, and their reformation due to the application of a pressure of 10 bars during 150ms with an exciting current of 350mA. The filtered and amplified sensed induced voltage is plotted below.

Considering that the drag force in the microchannel is important, the range of the pressure applied varies from 8 to 20 bars with a current range in the exciting coil from 350 to 1000 mA. In each measurement, the same procedure was followed. Initially, the current was applied in the exciting coil, the microscope camera started the recording at 15 fps, and no pressure was applied on the entry of the microchannel, thus the whole fluidic circuit was at atmospheric pressure, as the outlet of the microchannel was open. Then, a force was applied on the syringe during 150 ms, creating a flow of the MRF in the microchannel, as it was high enough to break the chains of particles.

In Fig. 6 four consecutive frames are presented, which depict the rupture of the chains of particles when the pressure was applied, followed by their reformation when the pressure was back to the atmospheric level. Below the frames, the filtered and amplified induced voltage signal is presented. By looking at the frames, it is clear that the chains of particles are broken in order to let the MRF flow until the particles form chains again. This change in the geometrical distribution of the ferromagnetic particles leads to a change of the magnetic

properties of the MRF, which, as described in the equation 8, leads to the creation of an induced voltage on the sensing coil. The voltage sensed is in the same reference as a source, thus, a positive induced voltage in the measurement corresponds to a decrease of the MRF permeance Λ_{mrf}. This result is explained by the role of the magnetic guide that is played by the particles. As these bridge-like structures are broken, the magnetic field B has passed through the oil of the MRF. The oil has a lower relative permeability compared to the ferromagnetic particles and a proportional decrease of flux is taking place in it.

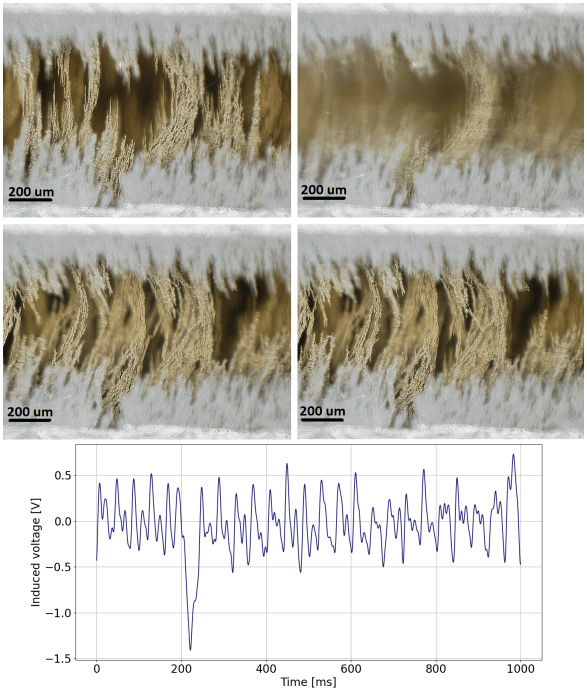

Fig. 7. Four frames of a video separated by 67ms each, which show the displacement of the chains of particles in the microchannel, and an increase of the concentration of the particles in the MRF due to the in-homogeneity of the fluid. A pressure of 10 bars is applied during 150ms with an exciting current of 1000mA. The filtered and amplified sensed induced voltage is plotted below.

In Fig. 7, four consecutive frames are recorded, which show a small flow of MRF that contrary to Fig. 6 is not created by breaking the chains of particles but by the slipping of the chains on the sides of the gap. A second effect showed in Fig. 7 is the increase of the ferromagnetic particles' concentration, due to the in-homogeneity of the MRF. As the chains guiding the magnetic field are not broken and the concentration of the particles increases, the magnetic properties of the MRF in the microchannel are improved and lead to an increase of the MRF permeance Λ_{mrf}. This is visible in the plot of the induced voltage, as the peak is in the opposite direction compared to the results in Fig. 6.

Both measured induced voltage from Fig. 6 and Fig. 7 were integrated from 160ms to 320ms, in order to calculate the variation of the MRF relative permeability through the equation 10. The results are presented in table III. In the case of Fig. 6, the particles are first agglomerated and the MRF has a relative permeability superior to the one calculated with the Maxwell-Garnett rule, then the chains of particles are broken and the distribution of the particles is chaotic, as seen in the second frame of the Fig. 6. Thus the Maxwell-Garnett rule criteria of particles' dispersion are met and the relative permeability μ_{mrf} can be approximated to 1.061. Using equation 10 would lead to a change of the relative permeability of the MRF from 1.112 to 1.061. In Fig. 7, since the particles remain agglomerated and not randomly dispersed in the fluid, the Maxwell-Garnett rule criteria are not met. For that reason, we only observe the distribution of the particles, the chains, and the changes the applied pressure brings about, without recalculating the new permeability. Finally, we observe that both in Fig. 6 and Fig. 7 the induced voltage contains frequency components in a period of around 20 ms, which corresponds to a frequency of 50 Hz. Thus, we can speculate that these components derive from the power supply instruments. In parallel, as the testing was performed in a room with other strong emitters of magnetic waves, like the electron microscope, they can also be accounted for the introduction of noise.

TABLE III
MEASUREMENTS OBTAINED THROUGH THE INDUCED VOLTAGE

Quantity	Value
Fig. 6 int V_i	6.603 * 10^{-6} Vs
Fig. 7 int V_i	-3.409 * 10^{-6} Vs
Fig. 6 $\Delta\mu_{mrf}$	-0.050841
Fig. 7 $\Delta\mu_{mrf}$	0.026248

IV. CONCLUSIONS

In this paper, we presented the design, fabrication, and experimental results of a microfluidic device for analyzing the properties of a MRF. The suggested setup simulated the conditions in the gap of a MR valve in terms of fluidic behaviour (pressure and flow rate) and electromagnetic behaviour. Its structure and choice of materials allowed the placement of the suggested device under an optical microscope, which was not possible with the traditional cylindrical structure of the annular magnetorheological valve. In this way, the behaviour of the particles under the application of a magnetic field was observed. The addition of a sensing coil allowed the induced voltage measurement and the comparison with the analytical equations. Thus, with this device, we achieved a better explanation of the experimental results with regard to induction phenomena in magnetorheological valves. The suggested analysis may further be exploited in MR valves that can act both for actuating but also for sensing purposes due to the induction phenomena.

ACKNOWLEDGMENT

The authors would like to thank the BRIDGE funding programme, conducted by the Swiss National Science Foundation (SNSF) and Innosuisse–Swiss Innovation Agency for the support.

REFERENCES

[1] J. Rabinow, "The magnetic fluid clutch," Electrical Engineering, vol. 67, no. 12, p. 1167-1167, 1948.

[2] A. G. Olabi, & A. Grunwald, "Design and application of magneto-rheological fluid," Materials & design, vol. 28, no. 10, p. 2658-2664, 2007.

[3] K. McDonald, L. Kinnicutt, A. M. Moran, & T. Ranzani, "Modulation of Magnetorheological Fluid Flow in Soft Robots Using Electropermanent Magnets," IEEE Robotics and Automation Letters (Early Access), 2022.

[4] R. Balak, & Y. C. Mazumdar, "Bistable Valves for MR Fluid-Based Soft Robotic Actuation Systems," IEEE Robotics and Automation Letters, vol. 6, no. 4, p. 8285-8292, 2021.

[5] S. Sassi, K. Cherif, L. Mezghani, M. Thomas, & A. Kotrane, "An innovative magnetorheological damper for automotive suspension: from design to experimental characterization," Smart Materials and Structures, vol. 14, no. 4, p. 811, 2005.

[6] T. H. Yang, et. al., "Magnetorheological Fluid Haptic Shoes for Walking in VR," IEEE Transactions on Haptics, vol. 14, no. 1, p. 83-94, 2020.

[7] R. Ahamed, S. B. Choi, & M. M. Ferdaus, "A state of art on magneto-rheological materials and their potential applications," Journal of Intelligent Material Systems and Structures, vol. 29, no. 10, p. 2051-2095, 2018.

[8] M. Ashtiani, S. H. Hashemabadi, & A. Ghaffari, "A review on the magnetorheological fluid preparation and stabilization," Journal of Magnetism and Magnetic Materials, vol. 374, p. 716-730, 2015.

[9] S. L. Ntella, et. al., "Preliminary Study of Pressure Self-Sensing Miniature Magnetorheological Valves," IEEE/ASME International Conference on Advanced Intelligent Mechatronics (AIM), pp. 606-611, IEEE, 2021.

[10] D. Grivon, Y. Civet, Z. Pataky, and Y. Perriard, "Detection of pressure or flow rate variations in MR valves through magnetic flux analysis," 19th International Conference on Electrical Machines and Systems (ICEMS), pp. 1-5, IEEE, 2016.

[11] S. Genç, & P. P. Phulé, "Rheological properties of magnetorheological fluids," Smart Materials and Structures, vol. 11, no. 1, 140, 2002.

[12] M. Ocalan, & G. H. McKinley, "Rheology and microstructural evolution in pressure-driven flow of a magnetorheological fluid with strong particle–wall interactions," Journal of Intelligent Material Systems and Structures, vol. 23, no. 9, p. 969-978, 2011.

[13] Suraj Sharadchandra Deshmukh, "Development, characterization and applications of magnetorheological fluid based 'smart' materials macro to micro scale," Doctoral dissertation, Massachusetts Institute of technology, United States of America, 2007.

[14] P. Domínguez-García, S. Melle, J. M. Pastor, M. A. Rubio, "Scaling in the aggregation dynamics of a magnetorheological fluid," Physical review E, vol. 76, no. 5, p. 051403, 2007.

[15] Nikon microscopy U, "Darkfield illumination," Nikon, accessed on 12 January 2022 (Online), available: https://www.microscopyu.com/techniques/stereomicroscopy/darkfield-illumination

[16] Amr I.Abdel-Fattah, Mohamed S.El-Genk, Paul W.Reimus, "On Visualization of Sub-Micron Particles with Dark-Field Light Microscopy," Journal of Colloid and Interface Science, vol. 246, no. 2, p. 410-412, 2002.

[17] LORD TECHNICAL DATA 2022, "MRF-132DG Magneto-Rheological Fluid," LORD, accessed on 14 January 2022 (Online), available: https://lordfulfillment.com/pdf/44/DS7015_MRF-132DGMRFluid.pdf

[18] A. Sihvola, "Electromagnetic mixing formulas and applications," IEEE Electromagnetic Waves Series, vol. 47, pp. 63-68, 1999.

[19] C. M. Lin, et al., "Trapping of bioparticles via microvortices in a microfluidic device for bioassay applications," Analytical chemistry, vol. 80, no. 23, p. 8937-8945, 2008.